



UNIVERSITY  
OF WOLLONGONG  
AUSTRALIA

University of Wollongong  
Research Online

---

Faculty of Engineering and Information Sciences -  
Papers: Part A

Faculty of Engineering and Information Sciences

---

2014

# Making a hydrophoretic focuser tunable using a diaphragm

Sheng Yan

*University of Wollongong, sy034@uowmail.edu.au*

Jun Zhang

*University of Wollongong, jz218@uowmail.edu.au*

Huaying Chen

*CSIRO Manufacturing Flagship*

Gursel Alici

*University of Wollongong, gursel@uow.edu.au*

Haiping Du

*University of Wollongong, hdu@uow.edu.au*

*See next page for additional authors*

---

## Publication Details

Yan, S., Zhang, J., Chen, H., Alici, G., Du, H., Zhu, Y. & Li, W. (2014). Making a hydrophoretic focuser tunable using a diaphragm. *Biomicrofluidics*, 8 (6), 064115-1 - 064115-12.

Research Online is the open access institutional repository for the University of Wollongong. For further information contact the UOW Library:  
[research-pubs@uow.edu.au](mailto:research-pubs@uow.edu.au)

---

# Making a hydrophoretic focuser tunable using a diaphragm

## **Abstract**

Microfluidic diagnostic devices often require handling particles or cells with different sizes. In this investigation, a tunable hydrophoretic device was developed which consists of a polydimethylsiloxane (PDMS) slab with hydrophoretic channel, a PDMS diaphragm with pressure channel, and a glass slide. The height of the hydrophoretic channel can be tuned simply and reliably by deforming the elastomeric diaphragm with pressure applied on the pressure channel. This operation allows the device to have a large operating range where different particles and complex biological samples can be processed. The focusing performance of this device was tested using blood cells that varied in shape and size. The hydrophoretic channel had a large cross section which enabled a throughput capability for cell focusing of  $\sim 15\,000$  cells  $s^{-1}$ , which was more than the conventional hydrophoretic focusing and dielectrophoresis (DEP)-active hydrophoretic methods. This tunable hydrophoretic focuser can potentially be integrated into advanced lab-on-a-chip bioanalysis devices.

## **Disciplines**

Engineering | Science and Technology Studies

## **Publication Details**

Yan, S., Zhang, J., Chen, H., Alici, G., Du, H., Zhu, Y. & Li, W. (2014). Making a hydrophoretic focuser tunable using a diaphragm. *Biomicrofluidics*, 8 (6), 064115-1 - 064115-12.

## **Authors**

Sheng Yan, Jun Zhang, Huaying Chen, Gursel Alici, Haiping Du, Yonggang Zhu, and Weihua Li

# Making a hydrophoretic focuser tunable using a diaphragm

Sheng Yan,<sup>1)</sup> Jun Zhang,<sup>1)</sup> Huaying Chen,<sup>2)</sup> Gursel Alici,<sup>1,3)</sup> Haiping Du,<sup>4)</sup>  
Yonggang Zhu<sup>2,5,a)</sup> and Weihua Li<sup>1,a)</sup>

<sup>1</sup>*School of Mechanical, Materials and Mechatronic Engineering University of Wollongong, Wollongong, NSW 2522, Australia.*

<sup>2</sup>*CSIRO Manufacturing flagship, Private Bag 10, Clayton South, VIC, 3169, Australia.*

<sup>3</sup>*ARC Centre of Excellence for Electromaterials Science, Innovation Campus, University of Wollongong, Wollongong, NSW 2500, Australia*

<sup>4</sup>*School of Electric, Computer and Telecommunication Engineering, University of Wollongong, Wollongong, NSW 2522, Australia*

<sup>5</sup>*Melbourne Centre for Nanofabrication/Australian National Fabrication Facility, 151 Wellington Road, Clayton, VIC, 3168, Australia*

Microfluidic diagnostic devices often require handling particles or cells with different sizes. In this investigation, a tunable hydrophoretic device was developed which consists of a PDMS slab with hydrophoretic channel, a PDMS diaphragm with pressure channel and a glass slide. The height of the hydrophoretic channel can be tuned simply and reliably by deforming the elastomeric diaphragm with pressure applied on the pressure channel. This operation allows the device to have a large operating range where different particles and complex biological samples can be processed. The focusing performance of this device was tested using blood cells that varied in shape and size. The hydrophoretic channel has a large cross section which enabled a throughput capability for cell focusing of  $\sim 15,000$  cells  $s^{-1}$ , which was more than the conventional hydrophoretic focusing and dielectrophoresis (DEP)-active hydrophoretic methods. This tunable hydrophoretic focuser can potentially be integrated into advanced lab-on-a-chip bioanalysis devices.

---

<sup>a)</sup> Author to whom correspondence should be addressed. Electronic mail: weihuali@uow.edu.au and yonggang.zhu@csiro.au

## I. INTRODUCTION

A large portion of the world's population has little or no access to quality healthcare, especially those who live in rural areas in developing countries. Being unable to access basic medical facilities like in urban medical centres could mean missing an early diagnosis and losing the best opportunity for treatment.<sup>1</sup> On this basis there is an obvious demand for affordable and portable diagnostic devices which can be performed at point-of-care or home by non-professional individuals<sup>2</sup>. Since microfluidics devices offer a variety of benefits, such as low sample volume, low cost, real-time detection, and greater portability; there has been an ever-increasing development in microfluidic platforms for point-of-care biomedical applications over the past decade<sup>3-5</sup>.

Many of the microfluidic diagnosis devices involve particle or cell separation. A number of techniques have been investigated for such a purpose, e.g., hydrodynamic filtration<sup>6-8</sup>, deterministic lateral displacement (DLD)<sup>9-13</sup> and so on<sup>14-16</sup>. The performance of these methods is dictated by a lateral length scale of the microchannel, named as critical diameter, in relation of the particle size. Yamada and Seki<sup>7</sup> first proposed the hydrodynamic filtration method for continuous particle separation using a microchannel having multiple side branch channels. Particles with a diameter larger than the critical diameter will not flow into the side channel whereas the smaller particles will. The critical diameter depends on the dimensions of the micro-channel, which in turn determines the size of particles to be filtered. The DLD, like the theoretical critical diameter, is another example, which was verified by experimental results<sup>9</sup>. It was found that if the diameter of a particle was less than the critical diameter, it would move in 'zigzag mode' and retain its position, whereas a particle with a diameter larger than the critical diameter behaved in the 'displacement mode', unlike smaller diameter particles. They will also have a shift angle which results in their being sorted from the mixture. The theory of DLD was further explored by Inglis *et al.*<sup>10</sup> and a model was presented to illustrate the effect that the micro-posts geometry has on the critical diameter for particle fractionation. Despite of the great effort, the hydrophoretic theory has not been fully established. The value of the critical diameter for particle separation is mainly determined empirically by analysing the experimental data<sup>17, 18</sup>. The main drawback of these methods is that the critical diameter is fixed for a given device. Once the channel has been fabricated, it cannot be easily modulated and thus limits the application to only particle samples with a narrow size range.

Tunable microfluidic devices are emerging to fill this gap due to the flexible nature of this design. Indeed, they have the potential to be controlled by a live feedback system, which uses experimental data to optimise the operating conditions and thus deliver the expected outcomes on time. A tunable elastomeric DLD device was first proposed by Beech and Tegenfeldt<sup>19</sup>. The distance between the micro-pillars was controlled by applying strain to the device, which altered the critical diameter. Chang and Cho<sup>20</sup> replaced the real pillar array with spot electrodes which could generate a virtual DLD array after AC

signals were applied. The ability to tune the critical diameter was achieved by changing the applied electric field. The combination of dielectrophoresis (DEP) and DLD was implemented by Beech *et al.*<sup>21</sup> using an insulator based DEP. The platinum wires inserted in the inlets and outlets of the DLD devices served as electrodes that generated a negative DEP force around the micro-posts. The critical diameter was tuned in the range of 2-6  $\mu\text{m}$  in a single device by altering the external AC signals. This combined technique could not only separate particles with regards to size, it could also polarise them. Besides, Choi and Park<sup>22</sup> also tried to make their hydrophoretic device tunable using the elastic deformation of polydimethylsiloxane (PDMS). Compressing the channel reduced its height and the critical diameter was then tuned from 7 to 2.5  $\mu\text{m}$ . Another way of tuning hydrophoresis by combining negative DEP with hydrophoresis was proposed by our group<sup>23,24</sup>. In this technique the critical diameter is controlled by manipulating the magnitude and frequency of AC signals. However, DEP-based devices do not work well with physiological media (conductivities  $>1 \text{ S m}^{-1}$ ), where cells become less polarisable than the medium<sup>25</sup>, which is why they usually operate in a low conductive medium.

To overcome these issues, we aimed to develop a new microfluidic focuser with a diaphragm that can adjust the height of the hydrophoretic channel when pneumatic pressure is applied. This will result in a robust, cost-effective, and buffer-compatible microfluidic device. The outline of this paper is as follows: Section 2 will introduce the materials and methods, including the methodology, design, and micro-fabrication, and the experimental setup and numerical simulation. The main results will be presented in Section 3, including the effect of the applied pressure, flow rate, and particle diameter on the focusing performance. Blood cells were introduced to test the capability of the tuneable hydrophoretic channel. The main conclusion will be drawn in Section 4.

## II. MATERIALS AND METHODS

### A. Methodology

A lab-on-a-chip device (Fig. 1) consists of a flow layer with a structured channel, a control layer with a rectangular cross section channel, and a glass slide. A sample can be introduced into the flow chamber in the flow layer that overlaps a lower fluid-filled control chamber. The two chambers are separated by a thin PDMS diaphragm that can be moved up or down by a pressure difference between the channels. The upper flow layer is a hydrophoretic device whose channel height can be tuned by stretching the elastomeric diaphragm. Typically, particles smaller than the critical diameter of the hydrophoretic channel will follow the rotation flow generated by the grooves and move back and forth and up and down (Fig. 1c). Given the appropriate pressure in the control layer, the diaphragm will stretch upwards, effectively reducing the height of the hydrophoretic channel. The critical diameter was decreased to a point where particles can form hydrophoretic ordering and be focused onto the sidewall of the channel (Fig. 1d). This developed approach overcomes the limitations of conventional

hydrophoretic devices whose critical diameter is pre-determined by the height of the channel once fabricated and is cost-effective compared with DEP-active hydrophoresis. Moreover, physiological media can also be injected into this channel, which has potential applications in processing cells.

## **B. Design and micro-fabrication**

The control chamber (1500  $\mu\text{m}$  wide, 40  $\mu\text{m}$  high and 10 mm long) was pre-filled with deionised (DI) water and connected to a pneumatic source. The flow chamber (500  $\mu\text{m}$  wide, 40  $\mu\text{m}$  high and 10 mm long) has one inlet and one outlet. Microposts were placed at the inlet to act like a filter, so most of debris can be prevented from entering the hydrophoretic channel. Crescent shaped grooves with a small curvature of 250  $\mu\text{m}$  and a large curvature of 300  $\mu\text{m}$  were patterned onto the top of the channel.

The hydrophoretic device was fabricated by two step photolithographic techniques, as reported in our previous work<sup>24</sup>. Briefly, a double layered mould was fabricated onto a 4" silicon wafer using SU-8 2050 (MicroChem Corp., Newton, MA). The first layer of photolithography was used as the main channel, and then the second layer with the pattern of grooves was laid on the first layer. The SU-8 2050 was spin-coated onto a clean silicon wafer in a three stage coating cycle (500 rpm for 20s, 2000 rpm for 20s, and 4000 rpm for 40s) to form a 40  $\mu\text{m}$  thick film. The wafer was then baked at 65 °C for 2 minutes and 95 °C for 7 minutes, before exposing it to UV light at a dose of 160  $\text{mJ cm}^{-2}$  under a chrome photomask on a mask aligner (SUSS MicroTec, Germany). Another two stage hard baking process (65 °C for 3 minutes and 95 °C for 7 minutes) was then carried out. After this the second photolithography was implemented onto the previous layer using the same procedures as the first layer. Afterwards, a two-layer photoresist was developed in the SU-8 developer (MicroChem Corp., Newton, MA) for 8 minutes and sequentially rinsed with acetone and isopropyl alcohol (IPA). The mould for control channel was fabricated using the same photolithographic technique as the first layer of hydrophoretic channel. All the moulds were treated with Trichloro(1h,1h,2h,2h perfluorooctyl)-silane (Sigma-Aldrich, Missouri, USA) to deposit a mono-layer of silane onto the surface to make the release of PDMS easy.

Sylgard 184 elastomer base and curing agent (Dow Corning Corporation, Midland, USA) were mixed evenly in a ratio of 10:1. The polydimethylsiloxane (PDMS) mixture was then poured onto the mold of flow layer and then totally degassed under a vacuum chamber. To fabricate the control layer, a mixture of uncured PDMS was spun onto the control channel mould at 200 rpm to form a 500  $\mu\text{m}$  thick film. Since the SU-8 mold was 40  $\mu\text{m}$  thick, the diaphragm on the top of the control channel was 460  $\mu\text{m}$  thick. All the PDMS were then baked at 65 °C for 2 h. The PDMS replica of the flow layer was peeled off the silicon wafer and inlet and outlet holes were punched with the tip of a custom made needle. After treating the

flow layer and control layer with plasma (PDC-002, Harrick Plasma, Ossining, NY) for 3 min, the hydrophoretic channel was sealed with the control layer. The control layer was then gently peeled from the silicon wafer because the thin film was fragile. Afterwards, a pneumatic inlet was punched through the flow layer and the control layer. The control layer was bonded to the glass slide after being treated by oxygen plasma, as mentioned above.

### **C. Material preparation**

Red fluorescent microparticles 8  $\mu\text{m}$  and 13  $\mu\text{m}$  in diameter, and green fluorescent beads 10  $\mu\text{m}$  (Thermo Fisher Scientific, USA) in diameter were used in our experiments. They were suspended in DI water, with Tween 20 (Sigma-Aldrich, Product No. P9416) added to this aqueous medium to impede the beads from sedimentation and aggregation. Samples of human blood were extracted from a healthy donor and then diluted 100 $\times$  (0.45% hct) in phosphate buffered saline (PBS) solution before being injected into the hydrophoretic channel.

### **D. Experimental setup**

A syringe pump (Legato 100, Kd Scientific) was used to inject the particle suspension into the micro-channel. The microfluidic device was placed under an inverted microscope (CKX41, Olympus, Japan) and the particle trajectories were captured by a CCD camera (Rolera Bolt, Q-imaging, Australia). An image processing program, Q-Capture Pro 7 (Q-imaging, Australia), was used to measure the focusing positions and the widths of the beads. Compressed air was provided by a 10<sup>6</sup> Pa air reservoir (Norgren Ltd, NSW, Australia) and was adjusted by a pressure regulator (AR30-02H, SMC Corp., Australia). This regulated air was then connected to the control layer.

### **E. Numerical simulation**

The channel deformation and particle trajectories were numerically modelled using the finite element software (COMSOL Multi-physics 4.3 COMSOL, Burlington, MA). To simulate channel deformation (Fig. 2a), a Solid Mechanics module that could calculate the strain of the elastic material under external forces was utilised to measure the displacement of the PDMS channel. Poisson's ratio and Young's modulus of PDMS were assumed to be 0.49 and 750 kPa, respectively<sup>22</sup>. The bottom of the control layer was set to be the fixed boundary condition. Air pressure of 1 bar was evenly distributed in the control chamber. The remaining walls were treated as free boundary conditions. To simulate particle trajectories, a 3 dimensional (3D) geometry of the deformed channel was built. The laminar flow module was first utilised to obtain the hydrodynamic characteristics inside the three dimensional model. A non-slip boundary condition was set for the channel walls, and the fluid was assumed to be incompressible. The flow rate at the inlet was set at 20  $\mu\text{l min}^{-1}$  and the pressure at the outlet was set at zero. The pressure and velocity vectors on the cross sections can be solved in the "Navier-Stokes Mode". The particle trajectories were then studied numerically in the particle tracing module. At the inlet, particles with a density and diameter of

1050 kg m<sup>-3</sup> and 10 μm respectively were released evenly along the width of the channel. Their movement in the channel were calculated 1.5 s with a calculation interval time of 10<sup>-4</sup> s, which provided smooth particle trajectories.

### III. RESULTS AND DISCUSSION

#### A. Modelling

Fig. 2a shows the deformed channel after a pressure of 1 bar was applied over the top wall of the pressure chamber. The top wall of the rectangular channel was deformed under this uniform air pressure. The diaphragm can be treated like slender beam that has the largest deformation in the middle, where a uniform load was applied onto the beam<sup>26</sup>. The deformation of the control layer was transferred to the flow layer, so the hydrophoretic channel was also deformed. To simplify the model, the grooves in the hydrophoretic channel were omitted. Deformation of the sidewall of the hydrophoretic channel was also omitted it was much less than the bottom wall. After measuring the relative deformation between the top wall and bottom wall, the height of the hydrophoretic channel was reduced by 12 μm at middle of the channel.

Fig. 2b illustrates the simulated particle trajectories in the deformed hydrophoretic channel that was built based on the previous simulation result of channel deformation shown in the Fig. 2a. The main channel was no longer rectangular because the bottom wall has a parabolic profile. After this deformation, smaller particles can satisfy the requirement for forming hydrophoretic ordering and after being released from the inlet, they followed the rotational flow generated by the grooves (Fig. 2b). Once they moved to the sidewalls a steric hindrance occurred which diffused them out of their helical streamlines and held them along the sidewalls; after which they gradually focused.

#### B. Effect of pressure

The use of a diaphragm between the hydrophoretic channel and the glass layer enabled the different focusing performance under various air pressures (Fig. 3). In this experiment, 10 μm diameter beads were injected into the hydrophoretic channel at a flow rate of 20 μl min<sup>-1</sup>. The particle trajectories in each image were captured after 100 μs of exposure, and the images were then superposed to better illustrate particle tracing. The original height of the hydrophoretic channel was 40 μm without any pressure applied, but the 10 μm beads could not form their hydrophoretic ordering according to the principle of hydrophoresis, and therefore the particles that were introduced at the inlet only migrated back and forth inside the channel (as shown in Fig. 3a). At the outlet, 10 μm particles could not be focused and evenly distributed across the width of the channel, but as air pressure applied it pushed the diaphragm upwards to a point where 10 μm particles satisfied hydrophoretic ordering and achieved hydrophoretic focusing (Fig. 3b). Then the steric hindrance could drive the particles along the sidewalls focus them into two lines at the outlet.

Fig. 3c shows the fluorescent profiles of particle trajectories under an applied pressure of 0.5 and 1.0 bar. The 10  $\mu\text{m}$  beads tended to move closer to the sidewalls as the air pressure increased, and they also became more focused. Obviously, a high pressure will reduce the height of the channel and therefore the particles will travel in a smaller space where the interaction between particles and grooves will be enough to focus them well. However, the pressure should not be high enough to cause the diaphragm to touch the top wall of hydrophoretic channel because this would cause the particles to block the middle of the channel. Most of them stuck at the edge of grooves and could not pass through the channel, but once the diaphragm was released, the trapped particles were flashed away by the fluid. This could also demonstrate that tunability was the best aspect of this device.

### C. Effect of flow rate

The dependence of tunable hydrophoretic focusing on the flow rate was characterised as the flow rate ranged from 10 to 100  $\mu\text{l min}^{-1}$  with pressure of 1 bar. 10  $\mu\text{m}$  diameter beads were introduced into the channel. The presence of the grooves was omitted, so the linear velocities of particles passing through the 500  $\mu\text{m}$  wide by 40  $\mu\text{m}$  high channel ranged from 0.83 to 8.33  $\text{cm s}^{-1}$ . Particles passing through a microfluidic channel normally experience inertial force and viscous force. Here, the particle Reynolds number  $R_p$  is the dimensionless ratio of particle inertia to the viscous force<sup>17</sup>, i.e.  $R_p = (\rho D^2 U) / (\mu D_h)$ , where  $\rho$  represents the fluid density,  $D$  is the particle diameter,  $U$  is the flow velocity,  $\mu$  is the dynamic fluid viscosity and  $D_h$  is the hydraulic diameter defined as  $D_h = 2WH / (W+H)$ . Where  $R_p > 1$ , particle inertia plays a dominant role and the equivalent paths of particles under hydrophoretic ordering are also affected by inertial force. However, the particle Reynolds number was 0.13 for 10  $\mu\text{m}$  beads at the maximum working flow rate of 100  $\mu\text{l min}^{-1}$  so in our experiments the particle inertial effect can be omitted.

Fig. 4a shows the focusing positions with various flow rates. The insets of Fig. 4a illustrate the optical images of particle trajectories at the outlet under a flow rate of 50 and 100  $\mu\text{l min}^{-1}$  respectively. The particles were focused onto the sidewalls of the channel with two separated lateral positions from 74.5 and 447.1  $\mu\text{m}$ , to 90.4 and 428.3  $\mu\text{m}$  with the flow rate varying from 10 to 100  $\mu\text{l min}^{-1}$ . Obviously, the flow rate had little effect on the focused position, which was consistent with the conclusion from Choi and Park<sup>18</sup>, who reported that particle position had no relationship with the flow rate.

The influence of flow rate on focused widths is shown in Fig. 4b. The focusing performance deteriorated as the flow rate increased, but when the flow rate was less than 50  $\mu\text{l min}^{-1}$ , the particles could still focus well and the focusing width of each streamline was within 40  $\mu\text{m}$ . Once the flow rate reached 100  $\mu\text{l min}^{-1}$ , particles deflected from sidewalls to the centreline of the channel with a larger focusing width. Since particles now passed through the channel faster at a higher flow rate, the

transverse flows were not strong enough to keep them migrating along the sidewalls. Moreover, the higher flow rate generated higher pressure inside the hydrophoretic channel, causing the pressure difference between the hydrophoretic channel and the pressure channel decrease. This means the diaphragm should not be pushed too high because poor focusing results were observed.

#### **D. Effect of particle diameter**

The influence of diameter on the focusing performance was examined by injecting particles with three different sizes, i.e., 8, 10, and 13  $\mu\text{m}$  in diameter at flow rate of  $20 \mu\text{L min}^{-1}$  into the hydrophoretic channel. Fig. 5a shows the focusing profiles of different particle diameters at the outlet with a pressure of 1 bar. Since the larger particles compared to the channel height could easily form hydrophoretic ordering, a narrower focusing profile was observed. As the air pressure increased from 0 to 1 bar, the focusing widths of particles with different diameters decreased rapidly (Fig. 5b). The focusing widths were reduced from 189 to 37  $\mu\text{m}$  for 8  $\mu\text{m}$  particles. A similar trend was observed for the 10  $\mu\text{m}$  beads where the focusing widths were 172, 72, 42, 24  $\mu\text{m}$  at 0, 0.5, 0.8, and 1.0 bar, respectively. The focusing width of 13  $\mu\text{m}$  beads reached 16  $\mu\text{m}$  at the maximum pressure, but as pressure inside the pressure channel rose and the pressure inside the hydrophoretic channel remained the same, the difference in pressure between the two channels increased. The diaphragm between the two layers went upwards to form a shallower hydrophoretic channel. Therefore, a good focusing performance was achieved at a high pressure.

#### **E. Focusing of blood cells**

Human blood is a complex biological fluid that contains red blood cells, platelets, white blood cells, and plasma. Typically, the diameters of spherical white blood cells have a large distribution from 7 to 30  $\mu\text{m}$  in size; red blood cells have a discoid shape and are 7 to 8  $\mu\text{m}$  in size, while discoid-shaped platelets are 2 to 4  $\mu\text{m}$  in size<sup>27</sup>. To examine whether our microfluidic device has the ability to focusing a complex sample that varies in shape and size, a blood sample diluted with a PBS (0.45% hct) buffer was injected into the channel; it should be noted that a concentration of blood cells will influence the focusing. Choi *et al.*<sup>28</sup> found that when the haematocrit of blood was higher than 1%, the interaction between cells and cells would not be negligible, that is, blood cells tend to flow adjacent to each other and cell to cell interaction will affect the focusing results. To avoid such an interaction, a diluted blood sample was prepared to improve the focusing of blood cells.

The optical micrograph in Fig. 6a shows the trajectories of blood cells at the outlet, in the absence of pressure. The blood cells were not focused in the micro-channel; they were distributed evenly at the outlet (see multimedia view Video 1). However, when a pressure of 1 bar was applied the blood cells focused onto the sidewalls (Fig. 6b), indeed, two separate streaks were observed near the sidewalls but blood cells were seldom seen in the middle area (see multimedia view Video 2).

After passing through the channel, most blood cells went through within a lateral range from 15 to 82  $\mu\text{m}$ , and 392 to 466  $\mu\text{m}$ , with a focusing behaviour similar to polystyrene beads; this result indicated that the tuneable hydrophoretic device could be used to focus blood cells.

The ability to throughput and focus blood cells was estimated to be approximately 15,000 cells  $\text{s}^{-1}$ , which was higher than conventional hydrophoretic focusing (6,667 cells  $\text{s}^{-1}$ )<sup>28</sup> and the DEP-active hydrophoretic approach (7,600 cells  $\text{s}^{-1}$ )<sup>24</sup>. To focus the disk-shaped red blood cells, the low throughput was attributed to the conventional 7.2  $\mu\text{m}$  high hydrophoretic channel combined with the smaller cross section<sup>28</sup>. Although the DEP-active hydrophoresis was another tunable microfluidic method, the working flow rate was normally low so that both large and small particles could be focused simultaneously<sup>24</sup>, but compared to the throughput of the inertial focuser (36,000 particles  $\text{s}^{-1}$ )<sup>29</sup>, this value was relatively low. However, this drawback can be overcome by parallelising multiple channels in a single chip.

#### **IV. CONCLUSIONS**

A tuneable hydrophoretic device was developed by inserting a diaphragm between the PDMS channel and the glass slide. This elastomeric diaphragm can be moved up and down by the pressure difference between the hydrophoretic channel and pressure channel; this movement, or deformation, was used to tune the height of hydrophoretic channel and thus change the critical focusing diameter; this meant that particles with the diameter smaller than the criterion of the hydrophoretic ordering can still be focused in the channel when air pressure was applied. A 3D model with the same geometry as the experimental channel was also built to simulate the deformation of the channels and particle trajectories. This model was then validated by the experimental data. The experimental results proved that particles with the diameter comparable to the height of the channel can still be focused in the smaller (deformed) channel by applying pressure onto the pressure channel. Particles can still be focused at a flow rate of 50  $\mu\text{L min}^{-1}$ . The throughput of the current device for focusing blood cells was estimated to be 15,000 cells  $\text{s}^{-1}$ , which is significantly higher than conventional hydrophoretic focusing and DEP-active hydrophoretic approaches. This tuneable device can focus particles with multiple diameters and complex biological samples in a single chip, and thus has great potential for applications such as miniaturised flow cytometry for cell counting and analysis.

#### **ACKNOWLEDGEMENTS**

This work is supported by the University of Wollongong -China Scholarship Council joint scholarships and the CSIRO Office of Chief Executive (OCE) Top-up Scholarship.

- <sup>1</sup>C. D. Chin, T. Laksanasopin, Y. K. Cheung, D. Steinmiller, V. Linder, H. Parsa, J. Wang, H. Moore, R. Rouse, G. Umvilighozo, E. Karita, L. Mwambarangwe, S. L. Braunstein, J. van de Wiggert, R. Sahabo, J. E. Justman, W. El-Sadr and S. K. Sia, *Nat. Med.*, **17**, 1015-1019 (2011).
- <sup>2</sup>Y. Nakashima, S. Hata and T. Yasuda, *Sens. Actuators, B*, **145**, 561-569 (2010).
- <sup>3</sup>Y. Rondelez, G. Tresset, K. V. Tabata, H. Arata, H. Fujita, S. Takeuchi and H. Noji, *Nat. Biotechnol.*, **23**, 361-365 (2005).
- <sup>4</sup>C. Ionescu-Zanetti, R. M. Shaw, J. Seo, Y. N. Jan, L. Y. Jan and L. P. Lee, *Proc. Natl. Acad. Sci. U. S. A.*, **102**, 9112-9117 (2005).
- <sup>5</sup>T. Thorsen, S. J. Maerkl and S. R. Quake, *Science*, **298**, 580-584 (2002).
- <sup>6</sup>M. Yamada and M. Seki, *Anal. Chem.*, **78**, 1357-1362 (2006).
- <sup>7</sup>M. Yamada and M. Seki, *Lab Chip*, **5**, 1233-1239 (2005).
- <sup>8</sup>M. Yamada, M. Nakashima and M. Seki, *Anal. Chem.*, **76**, 5465-5471 (2004).
- <sup>9</sup>L. R. Huang, E. C. Cox, R. H. Austin and J. C. Sturm, *Science*, **304**, 987-990 (2004).
- <sup>10</sup>D. W. Inglis, J. A. Davis, R. H. Austin and J. C. Sturm, *Lab Chip*, **6**, 655-658 (2006).
- <sup>11</sup>B. R. Long, M. Heller, J. P. Beech, H. Linke, H. Bruus and J. O. Tegenfeldt, *Physical Review E*, **78** (2008).
- <sup>12</sup>J. P. Beech, *Lab Chip*, **9**, 2698 (2009).
- <sup>13</sup>J. McGrath, M. Jimenez and H. Bridle, *Lab Chip*, **14**, 4139-4158 (2014).
- <sup>14</sup>S. Choi, O. Levy, M. B. Coelho, J. M. S. Cabral, J. M. Karp and R. Karnik, *Lab Chip*, **14**, 161-166 (2014).
- <sup>15</sup>D. Di Carlo, J. F. Edd, D. Irimia, R. G. Tompkins and M. Toner, *Anal. Chem.*, **80**, 2204-2211 (2008).
- <sup>16</sup>D. Di Carlo, *Lab Chip*, **9**, 3038-3046 (2009).
- <sup>17</sup>S. Choi, S. Song, C. Choi and J.-K. Park, *Anal. Chem.*, **81**, 50-55 (2009).
- <sup>18</sup>S. Choi and J.-K. Park, *Lab Chip*, **7**, 890-897 (2007).
- <sup>19</sup>J. P. Beech and J. O. Tegenfeldt, *Lab Chip*, **8**, 657-659 (2008).
- <sup>20</sup>S. Chang and Y.-H. Cho, *Lab Chip*, **8**, 1930-1936 (2008).
- <sup>21</sup>J. P. Beech, P. Jonsson and J. O. Tegenfeldt, *Lab Chip*, **9**, 2698-2706 (2009).
- <sup>22</sup>S. Choi and J.-K. Park, *Lab Chip*, **9**, 1962-1965 (2009).
- <sup>23</sup>S. Yan, J. Zhang, M. Li, G. Alici, H. Du, R. Sluyter and W. Li, *Sci. Rep.*, **4** (2014).
- <sup>24</sup>S. Yan, J. Zhang, G. Alici, H. Du, Y. Zhu and W. Li, *Lab Chip*, (2014).
- <sup>25</sup>S. Park, Y. Zhang, T.-H. Wang and S. Yang, *Lab Chip*, **11**, 2893-2900 (2011).
- <sup>26</sup>W. Beattie, X. Qin, L. Wang and H. Ma, *Lab Chip*, **14**, 2657-2665 (2014).
- <sup>27</sup>M. Kersaudy-Kerhoas and E. Sollier, *Lab Chip*, **13**, 3323-3346 (2013).
- <sup>28</sup>S. Choi, S. Song, C. Choi and J. K. Park, *Small*, **4**, 634-641 (2008).
- <sup>29</sup>A. J. Chung, D. R. Gossett and D. Di Carlo, *Small*, **9**, 685-690 (2013).

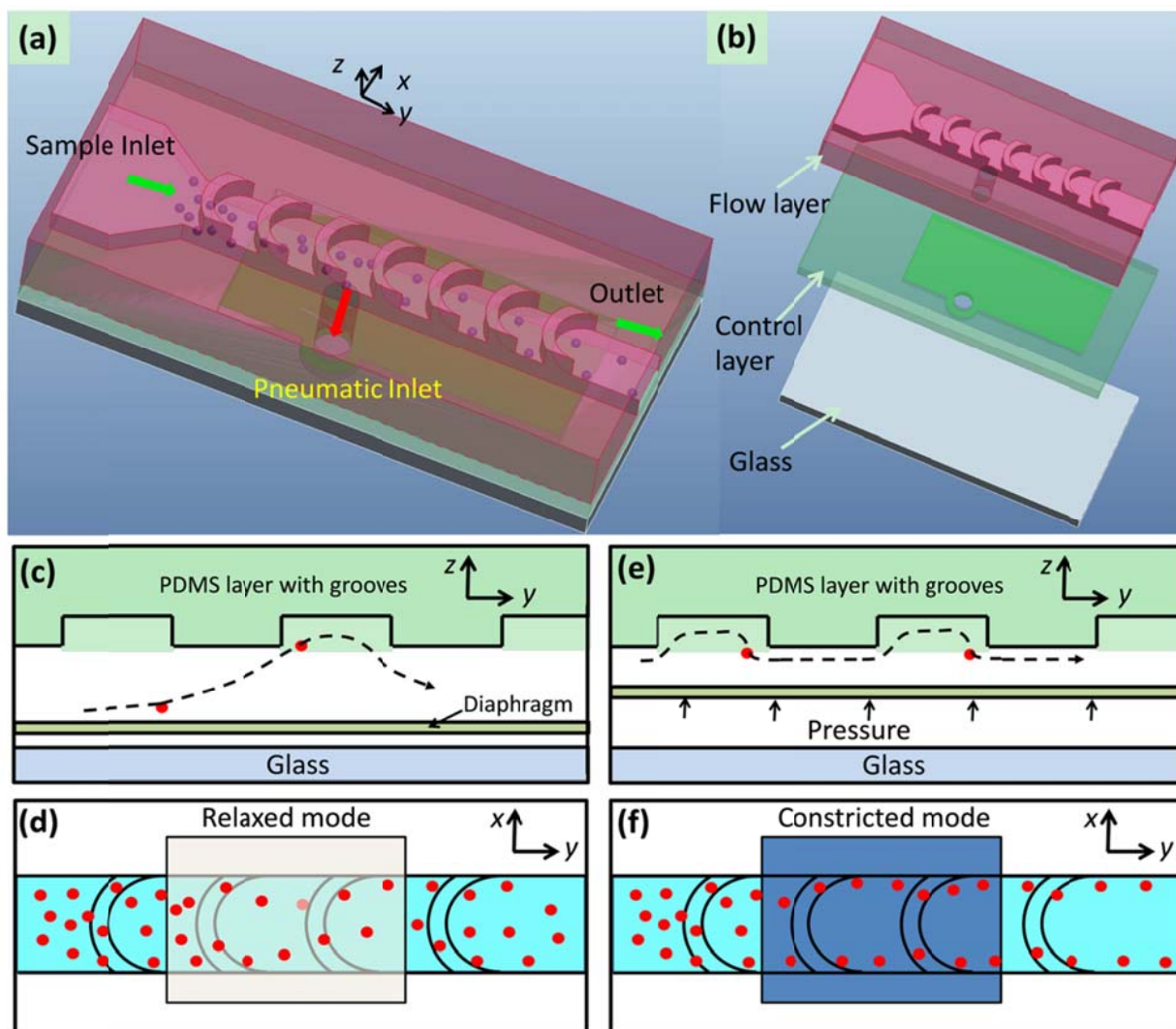


FIG. 1. (a) Overview of tuneable hydrophoretic focuser, (b) Exploded view of tunable focuser. The device consists of a flow layer, a control layer, and a glass slide. Cell or particle suspension flows through the upper channel, while the lower channel is connected to a pressure source. The two channels are separated by a thin diaphragm. Section views show the effective height of the upper channel in relaxed mode (c) and constricted mode (e). (d) Top view shows that particles without hydrophoretic ordering move back and forth in the channel. (f) After applying pressure on the diaphragm, the upper channel height is reduced. The particles are easy to satisfy the hydrophoretic ordering in the constricted channel and be focused along the sidewalls of the channel.

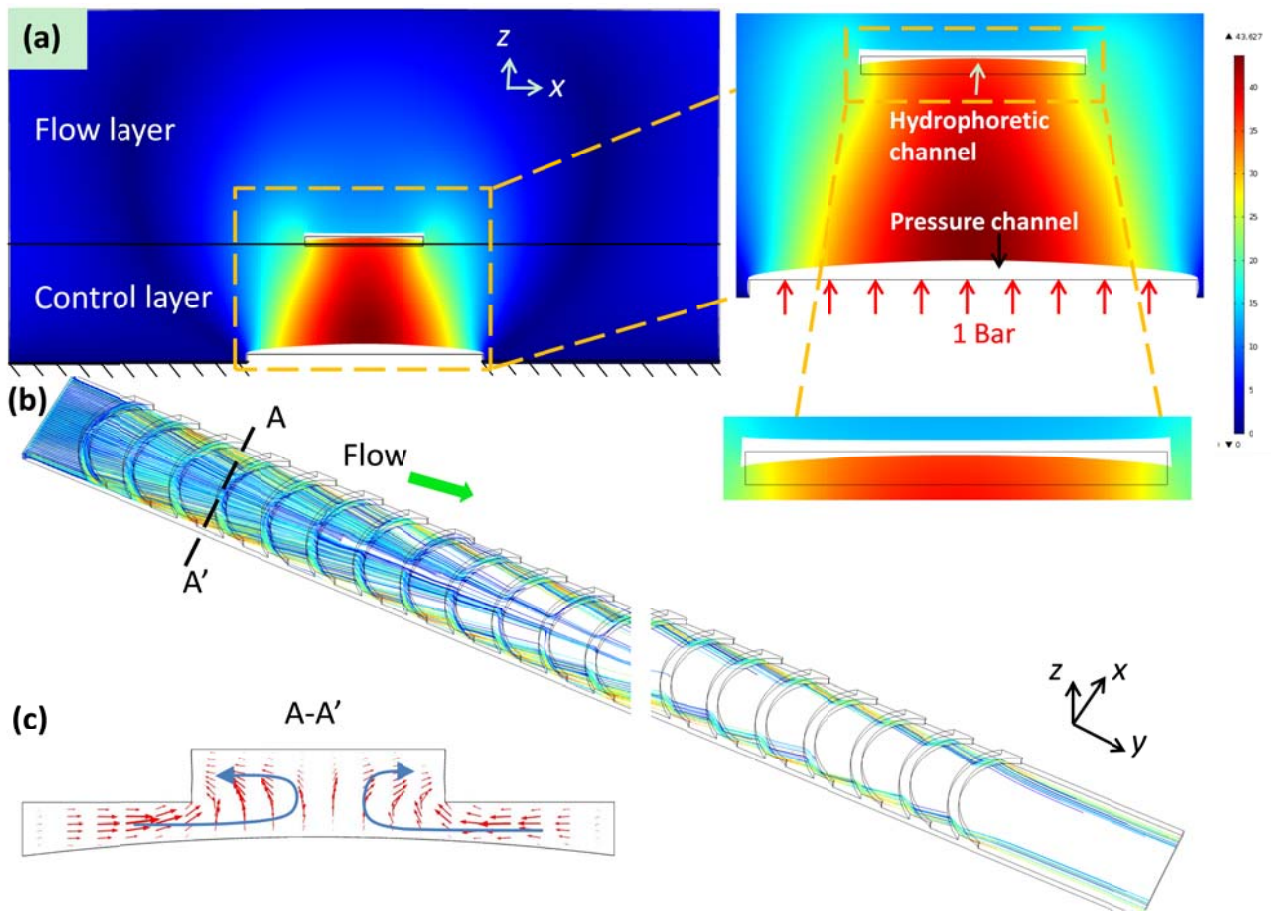


FIG. 2. (a) Simulation results of channel deformation induced by e air pressure. The wire frame represents the initial shape/position and the deformed shape is coloured using the scale bar to illustrate total displacement of the PDMS channel. Red represents a large displacement and blue represents a small displacement. (b) Numerically predicted particle trajectories in two sections of the micro-channel. The steric effect makes the particles diffuse out of convective vortices and assume hydrophoretic ordering. The image on the left shows the entrance section of the channel and the image on the right show the exit section. The colour of the trajectories denotes particle velocity. Red represents high speed and blue represents low speed. (c) The calculated results of flow field in the cross section of the deformed channel along the line, A-A'. Two convective vortices were generated by grooves.

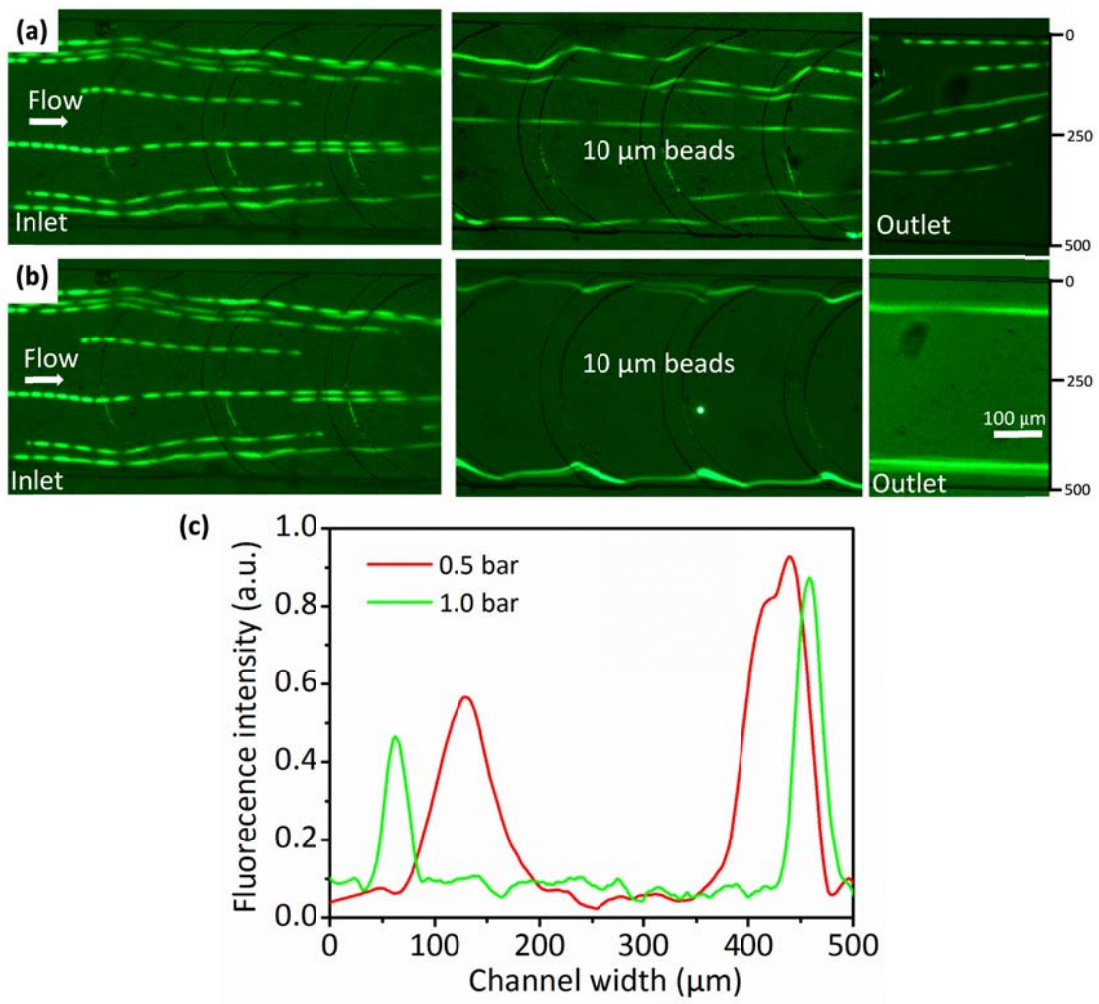


FIG. 3. Experimentally focused patterns of 10  $\mu\text{m}$  particles at various air pressure. The applied flow rate was  $20 \mu\text{l min}^{-1}$ . Beads were introduced evenly at the inlet. The microscopy images show the trajectories of particles along the whole channel at an air pressure of 0 bar (a) and 1 bar (b). (c) Measured fluorescence profiles of particle trajectories.

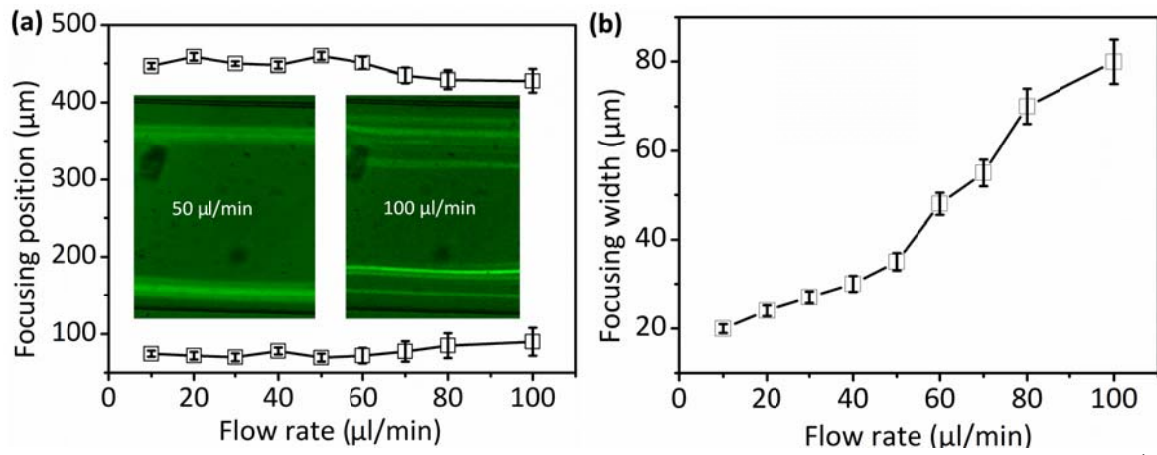


FIG. 4. Measured focused positions (a) and focused widths (b) from the fluorescent profiles. The flow rate was changing from 10 to 100  $\mu\text{l min}^{-1}$  and the applied pressure was 1 bar. The insets showing the focusing patterns of particles at the outlet at the flow rate of 50 and 100  $\mu\text{l min}^{-1}$ , respectively. The average value was 3 times the measurement.

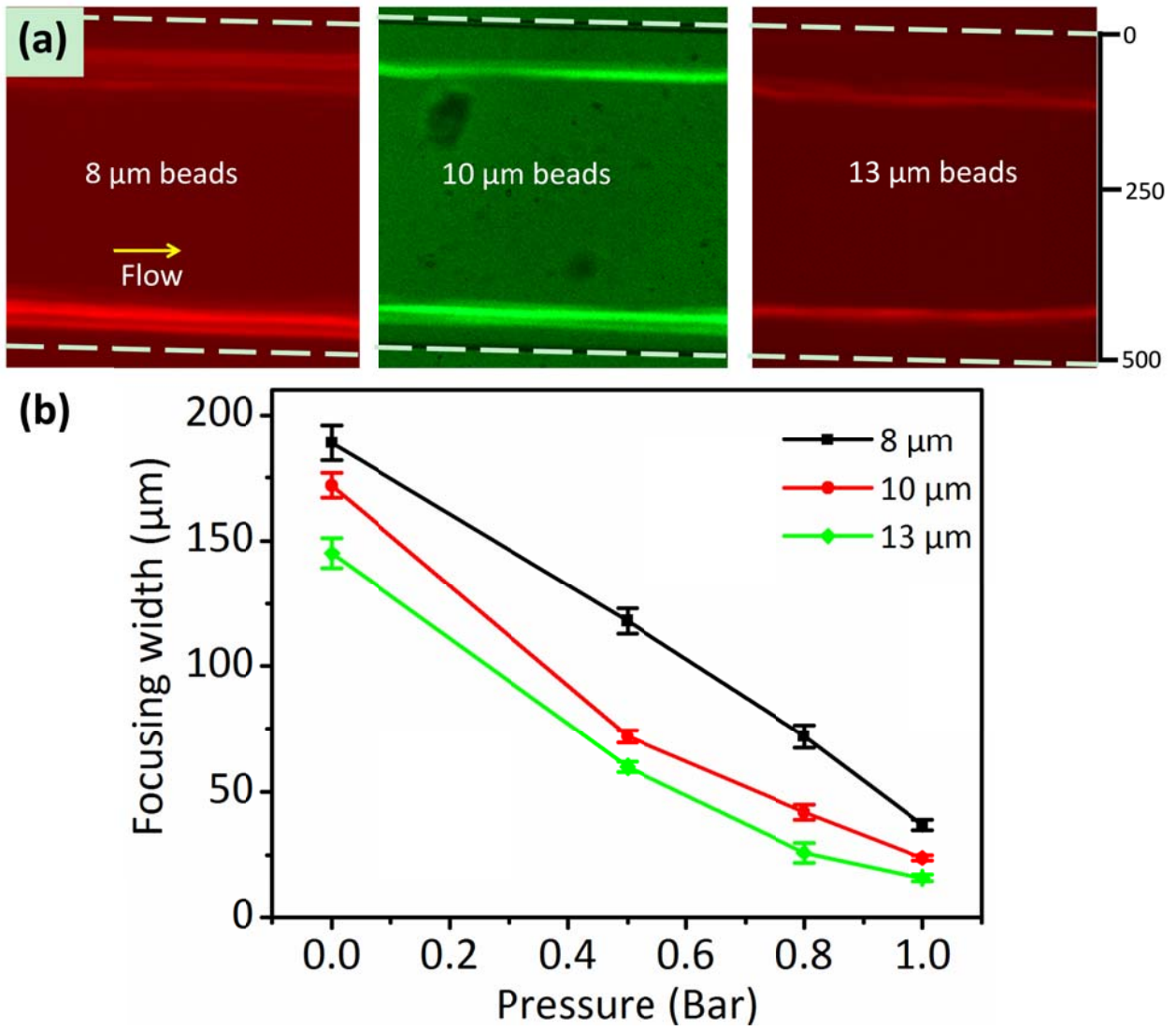


FIG. 5. (a) Optical micrographs showing the focusing patterns of 8, 10, and 13  $\mu\text{m}$  beads at the outlet. The applied pressure was 1 bar and the flow rate was  $20 \mu\text{L min}^{-1}$ . (b) Measured focused widths from the fluorescent profiles. The average value was 3 times the measurement.

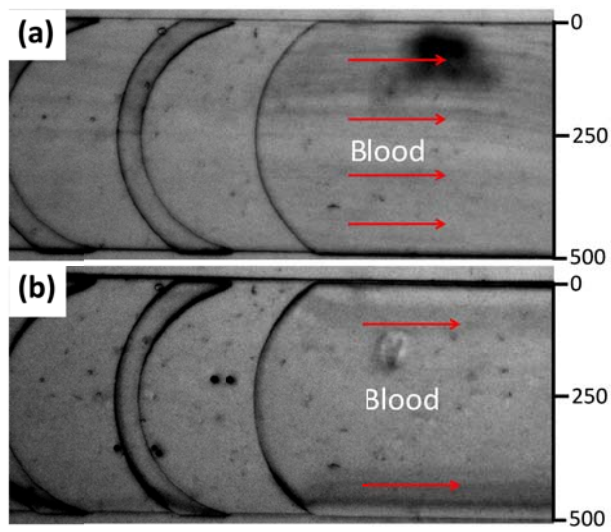


FIG. 6. Focusing patterns of blood cells at the outlet. The flow rate was  $20 \mu\text{l min}^{-1}$ . (a) The microscopy image shows that the cells were distributed evenly at the outlet after passing through the hydrophoretic channel without pressure. (b) Optical image showing cells were focused along the sidewalls of the channel with a pressure of 1bar. (Multimedia view)